J. Phys. B: At. Mol. Opt. Phys. 26 (1993) 3559–3572. Printed in the UK

Sm L-subshell ionization probabilities and alignment as a function of the impact parameter for 1 MeV proton impact

R Dörner†, K Ullmann†, J Euler†, R Koch†, I Legrand‡, R Seip†, J Ullrich§ and H Schmidt-Böcking†

† Institut für Kernphysik, Universität Frankfurt, D6000 Frankfurt, Federal Republic of Germany

‡ CERN, CH1211 Geneva, Switzerland

§ GSI, D6100 Darmstadt, Federal Republic of Germany

Abstract. For 1 MeV p → Sm the impact parameter dependence of the L-subshell ionization and of the alignment parameters A_{20} and A_{22} have been measured. For the spherically symmetrical L_I-subshell good agreement with standard SCA and coupled channel calculations has been observed. For the L_{II}-, L_{III}-subshell and the alignment parameters, however, severe deviations from the theoretical predictions within the SCA approach have been found. As a possible reason for these discrepancies a quasi-adiabatic adjustment of wavefunction to the rotating internuclear axis is discussed.

1. Introduction

Inner-shell ionization by swift ion impact has been extensively studied from the experimental as well as from the theoretical side. Experimental total cross sections for K- and L-shell ionization in very asymmetric collisions ($Z_{projectile} \ll Z_{target}$) are satisfactorily described by first-order theories like SCA if the correct trajectories, relativistic effects, and the recoil of the target nucleus are taken into account (Hansteen *et al* 1985). However, total cross section measurements are not a very sensitive test for ionization theories.

Studies of the impact parameter dependence of K-shell ionization were able to deliver a stringent test for higher-order corrections like Coulomb deflection, Coulomb repulsion and the binding effect (Schmidt-Böcking *et al* 1977, 1982, Andersen *et al* 1976, 1982). They could in particular prove the influence of the target recoil on the ionization process (Dost *et al* 1981, Schmidt-Böcking *et al* 1982, Gruber 1983, Cheng-ming Fou *et al* 1983, Steinbauer and Benka 1989, Bräuning *et al* 1991). This recoil effect can easily be included in the basic concept of SCA (Rösel *et al* 1982). For the L-shell, however only a few experimental results are so far available on the impact parameter dependence of the ionization probability. (Laegsgaard *et al* 1974, Stiebing *et al* 1976, Andreamonje *et al* 1981, Konrad *et al* 1984, Nolte *et al* 1984, Berinde *et al* 1984, Ullrich *et al* 1986, Dexheimer *et al* 1986, Zehendner *et al* 1987, Schadt *et al* 1988). They demonstrated the importance of relativistic effects for the ionization probability of the L_I-subshell (Ullrich *et al* 1986) and could in particular unambiguously prove the important higher-order effect of mixing of the L-subshells (Dexheimer *et al* 1986, Schadt *et al* 1988, Zehendner *et al* 1987). Even for a system as asymmmetric as 0.9 MeV Ne^{3+} → Yb (Dexheimer *et al* 1986) and 4 MeV p → Sm (Zehendner *et al* 1987) a distribution of the L-vacancies corresponding to the statistical weights of the substates was found for all impact parameters. This highlighted the limitations of first-order theories like SCA. Coupled channel calculations which include at least transitions between the subshells were necessary to describe the data (Legrand

0953-4075/93/203559+14$07.50

et al 1992). Using different projectile charges but the same impact velocity Dexheimer and co-workers (1986) showed that this vacancy sharing between the L-subshells strongly depends on the perturbation strength (see table 1). Therefore in this work we chose a very asymmmetric collision system with a perturbation strength smaller than in all previous experiments. The aim was to avoid the mixing between the L-subshells and to assure ideal conditions for the application of perturbation theory. This experiment should then also deliver a sensitive test for another interesting effect, which is the adiabatic rotation of the electronic states during the collision.

For the ionization of a non-spherical symmetric subshell like the $L_{II,III}$-subshell, it is not obvious from first principles how the magnetic substates are oriented in the laboratory frame. Most theoretical approaches so far use the incident beam axis as a quantization axis for the magnetic substates and keep this orientation of the atomic orbitals frozen during the collision process (Jakob 1985). Probably for very fast collisions ($v_p/v_e \gg 1$, with v_e being the classical orbital velocity of the electron and v_p being the projectile velocity) this assumption of complete non-adiabaticity of the collision process is well founded. But for v_p/v_e getting smaller the target atomic wavefunctions get more and more time to adiabatically adapt to the dynamically changing two-centre potential. The monopole part of this adiabatic effect on innershell ionization has been well known for many years as binding effect (Brandt *et al* 1966). It is well established that for close collisions, i.e. impact parameters smaller than the classical shell radius, the binding energy of the united atom ($Z_P + Z_T$) instead of the pure target binding energy has to be used in the SCA calculations. For K-shell ionization of Ti by p impact even a time dependent binding energy had to be introduced into the SCA in order to obtain agreement with the experimental data (Bräuning *et al* 1991). If now even the radius and binding energy of the atomic shells dynamically adapt to the changing potential during the collision it cannot be expected that the angular orientation of a non-isotropic wavefunction will stay unaffected. Since there are no significant external fields the only symmetry axis of the potentials is the internuclear axis between projectile and target nucleus. For small scattering angles the internuclear axis almost coincides with the beam axis long before and after the collision. For $t = \pm\infty$ one can therefore assume the beam axis to be the quantization axis for the initial and final states. During the collision however the internuclear axis rotates. The angular velocity of this rotation depends on the impact parameter. Therefore it is still an open question in which region the common assumption of wavefunctions with a quantization axis frozen along the beam axis is reasonable. This will depend on the ratio of v_p/v_e and on the impact parameter. The picture of a completely non-adiabatic collision with 'frozen orbitals' or the complementary picture of a completely adiabatic collision with 'rotating orbitals' (as used in all MO calculations) mark only the two extremes. Hansen and co-workers (1990) demonstrated by a coupled channel calculation for electron capture in nearly adiabatic collisions the feature of a *slippage phenomenon*, i.e. that the major axis of the 2p charge state density lags behind the internuclear axis. For further discussion see also the comment of Salin (1990). Legrand and co-workers (1991) adapted this concept to SCA calculations of inner-shell ionization.

L-subshell ionization probabilities and especially the alignment are well suited for a study of these effects. The ionization probability for the L_{II}- and the L_{III}-subshell in the case of 'frozen orbitals' should be much different from those in the case of 'rotating orbitals' since the overlap of the flight path of the projectile with the electron cloud is very different in both cases. Figure 1(*a*) shows schematically the path for 'frozen orbitals' seen from the target frame, which is in this case identical to the laboratory frame. For 'rotating orbitals' the path seen in the target system (i.e. the rotating system) is shown in figure 1(*b*). In this case the quantization axis is at all times identical to the internuclear axis.

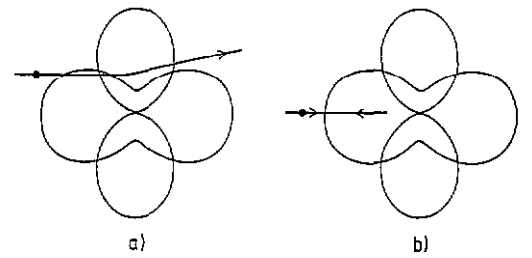

Figure 1. Path of the projectile through the target wavefunctions seen from the target system (schematically) see text. (*a*) 'Frozen orbitals', the quantization axis is aligned along the beam axis. (*b*) 'Rotating orbitals', the quantization axis rotates with the internuclear axis. Note that in this case the target system is rotating against the laboratory system. Therefore the path looks for all impact parameters similar to the path for impact parameter zero.

To investigate these effects for the L-subshell ionization, we have measured the impact parameter dependence of the $L_{I,II,III}$-subshell ionization probability and of the alignment of the L_{III}-shell for 1 MeV proton impact on samarium. The aim of this work is to explore the limitations of semiclassical approaches like SCA or coupled channel calculations.

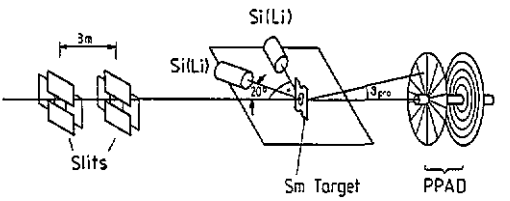

Figure 2. Experimental set-up.

2. Experiment and data reduction

The experiment was performed at the 2.5 MV Van de Graff accelerator of the Institut für Kernphysik in Frankfurt. The experimental set-up is shown in figure 2. The proton beam is collimated to a divergence less than 4 mrad. It hits a thin target of 100 mg cm^{-2} Sm evaporated on 10 mg cm^{-2} carbon backing. The target is thin enough that (a) projectile double scattering is negligible for the large scattering angles under investigation and (b) x-ray reabsorption in the target is very small (Bauer *et al* 1978). The unscattered protons are dumped in a Faraday cup, while the scattered particles are detected by a parallel plate avalanche detector (PPAD). This detector has two position sensitive layers. The first anode is divided into 16 sectors to determine the scattering plane for the alignment measurement, the second has 14 concentric rings to measure the scattering angle. Each sector and ring is read out separately by a fast amplifier followed by a constant fraction discriminator to handle particle rates of more than 10^6 Hz. The measured scattering angles are converted into impact parameters assuming an unscreened Coulomb potential. For the largest impact parameter measured in this experiment of 3300 fm the difference in the scattering function between a screened and an unscreened potential is below 5% (Hagmann *et al* 1982). In order to cover a broad range of impact parameters the experiment was performed with three different detector target distances. The beam current was reduced to obtain a count rate

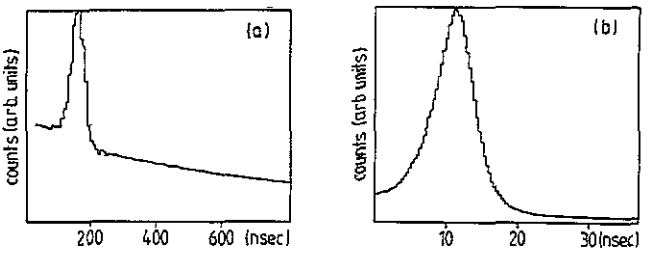

Figure 3. (*a*) Time spectrum for the coincidence between x-ray and ring anode of the PPAD (linear ordinate). (*b*) Time-amplitude spectrum for the coincidence between the sector and ring anode of the PPAD (linear ordinate).

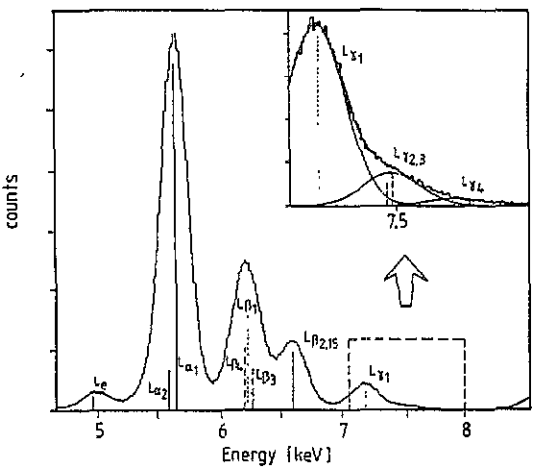

Figure 4. Sm L-x-ray spectrum. Full lines show transitions leading into the L_{III}-subshell, dotted lines show transitions into the L_{II}-subshell and broken lines transitions into the L_I-subshell.

below 3 MHz on the PPAD. The x-rays are detected with two Si(Li) detectors, one with an energy resolution of 180 eV FWHM at 5 keV the other with 210 eV FWHM. They were mounted in one plane with 90° and 20° with respect to the beam axis. Between the Si(Li), ring and sector part of the PPAD a triple coincidence had to be made. One time-to-amplitude converter (TAC) is started by the signals of any of the Si(Li) detectors and stopped by the signals from the ring anode of the PPAD (see figure 3(*a*)). A second TAC is started by the signals from the sector anode and stopped by the signal from the ring anode of the PPAD (see figure 3(*b*)). For the x-ray projectile coincidence the time resolution was mainly determined by the collection time of the Si(Li) detector and was therefore dependent on the x-ray enrgy. A time resolution of 38 ns FWHM for the Sm L_l-line (4.9 keV) and about 18 ns FWHM for the L_γ-group (< 7 keV) was achieved. The electronic set-up for this experiment is discussed in detail in (Schmidt-Böcking *et al* 1983). An x-ray spectrum obtained from one of the Si(Li) detectors is shown in figure 4.

2.1. Ionization probabilities

The L-subshell ionization probabilities $I_{L_i}(b)$ were calculated from the x-ray emission probabilities for the L_α line (transition $3d \rightarrow 2p_{3/2}$), for the $L_{\gamma_{2,3,4}}$ line (transition $4p \rightarrow 2s$ and $5p \rightarrow 2s$) and for the L_{γ_1} line (transition $4d \rightarrow 2p_{1/2}$) using

$$I_{L_I}(b) = P_{L_{\gamma 2,3,4}}(b)\frac{1}{\omega_I}\frac{\Gamma_I}{\Gamma_{I,\gamma 2,3,4}} \tag{1}$$

$$I_{L_{II}}(b) = P_{L_{\gamma_1}}(b)\frac{1}{\omega_2}\frac{\Gamma_{II}}{\Gamma_{II,\gamma_1}} - I_{L_I}(b) f_{12} \tag{2}$$

$$I_{L_{III}}(b) = P_{L_\alpha}(b)\frac{1}{\omega_3}\frac{\Gamma_{III}}{\Gamma_{III,\alpha}} - I_{L_{II}}(b) f_{23} - I_{L_I}(b)(f_{12}f_{23} - f_{13}). \tag{3}$$

The decay rates Γ_i are taken from (Scofield 1974), the Coster–Kronig transition coefficients f_{ij} and the fluorescence yields ω_i are taken from (Krause 1979). The quoted accuracy of the ω_i is 5% and 15% for the f_{ij}. The absolute x-ray emission probabilities $P_{L_x}(b)$ are given by

$$P_{L_x}(b) = \frac{N_{L_x}(b)}{N_P(b)}\frac{4\pi}{\Delta\Omega_x(E_x)} \tag{4}$$

$N_{L_x}(b)$ is the number of true coincidences of an x-ray in the L_x line with a scattered proton with impact parameter b. The effective Si(Li) solid angle $\Delta\Omega_x(E_x)$ was measured with an accuracy of ±9%. In order to measure the total number of scattered particles $N_P(b)$ to a certain impact parameter the pulses of a random pulser with rate λ_P were fed into the test input of one of the Si(Li) pre-amplifiers. From the number of random coincidences ΔN_{dt} between these pulser pulses and the scattered particles during a certain time interval Δt $N_P(b)$ was calculated with

$$N_P(b) = \frac{\Delta N_{dt}}{\lambda_P \Delta t}. \tag{5}$$

These pulses are processed by the same electronics as the real x-ray pulses. Therefore this random sample measurement of $N_P(b)$ is affected by exactly the same electronic deadtime as the true coincidences $\Delta N_{L_x}(b)$. This is of great importance because of the high projectile count rates which were necessary for this experiment. The error of this determination of $N_P(b)$ is negligible since λ_P and Δt are known very precisely.

As can be seen in figure 4 the $L_{\gamma 2,3,4}$ line can not be well resolved with Si(Li) detectors. Therefore $P_{L_{\gamma 2,3,4}}(b)$ was extracted in two steps. First the relative b dependence was determined by analysing only the part >7.5 keV of the spectrum. This part is not contaminated by any other unresolved line and thus the shape of the b dependence can be well determined. In a second step we analysed which fraction of the $L_{\gamma 2,3,4}$ falls into the chosen window >7.5 keV by unfolding the lines as shown in figure 4. Due to this unfolding procedure the absolute value of $P_{L_{\gamma 2,3,4}}$ has an additional error of ±20%.

From the errors discussed so far the systematical error of the absolute values is calculated to be ±30% for $I_{L_I}(b)$ and ±20% for $I_{L_{II}}(b)$ and $I_{L_{III}}(b)$.

2.2. Alignment

The alignment tensor components A_{20} and A_{22} can be obtained from the angular distribution of the radiative transitions (Berezkho and Kabachnik 1977, Blum and Kleinpoppen 1979). For the special case of a transition into the L_{III}-subshell the x-ray intensity $I(b, \vartheta, \phi)$ at a given impact parameter b, polar angle ϑ and azimuthal angle ϕ is given by:

$$I(b,\vartheta,\phi) = \frac{P_0}{4\pi}\Big[1 + \sqrt{\tfrac{3}{2}}\alpha_2 A_{22}(b)\sin^2\vartheta\cos 2\phi - \sqrt{\tfrac{3}{2}}\alpha_2 A_{21}(b)\sin 2\vartheta\cos\phi + \tfrac{1}{2}\alpha_2 A_{20}(b)\left(3\cos^2\vartheta - 1\right)\Big]\mathrm{d}\vartheta\,\mathrm{d}\phi. \tag{6}$$

The anisotropy coefficients α_2 for the different transitions can be found in (Berezkho and Kabachnik 1977). It is $\alpha_2 = 0.5$ for the L_l line which was used for the alignment measurement in this experiment. Equation (6) is valid in any coordinate frame independent of its orientation with respect to the laboratory system. One should note that the alignment tensor components are dependent on the reference frame chosen for the angles ϑ and ϕ. For simplicity we decided on the laboratory frame where the z-axis is the beam axis and θ is the polar angle with respect to the beam axis. As already discussed in the introduction this is not necessarily the natural reference frame for the target atomic orbitals. Using the laboratory system for the data analysis does not mean that the alignment parameters extracted this way are by any means model dependent. These parameters $A_{KQ}^{\text{lab}}(b)$ measured in the laboratory frame can be easily transformed to any rotated frame using the rotational matrices.

By integrating equation (6) over the azimuthal angle one obtains:

$$I(b,\vartheta) = \tfrac{1}{2}P_0\left[1 + A_{20}^{\text{lab}}(b)\left(\tfrac{3}{4}\cos^2\vartheta - \tfrac{1}{4}\right)\right]\mathrm{d}\vartheta. \tag{7}$$

The alignment parameter A_{20}^{lab} can then be obtained by measuring the L_l x-ray intensity at different polar angles ϑ integrated over all azimuthal angles ϕ (i.e. neglecting the information of the sector part of the PPAD). We choose $\vartheta = 90°$ as our reference angle. A_{20}^{lab} can then be determined as follows:

$$A_{20}^{\text{lab}}(b) = \frac{\left[I(b,\vartheta)/I(b,\vartheta = 90°)\right] - 1}{\tfrac{3}{4}\cos^2\vartheta - \tfrac{1}{4} + \tfrac{1}{4}\left[I(b,\vartheta)/I(b,\vartheta = 90°)\right]}. \tag{8}$$

To determine the ratio $I(b,\vartheta)/I(b,\vartheta = 90°)$ experimentally the ratio of solid angles and detection efficiencies of the two Si(Li) detectors has to be known. This was measured using a vanadium target instead of the Sm. The isotropic V K_α line has nearly the same energy as the Sm L_l line.

A vacancy in the L_{III}-subshell can not only be produced by knocking out an electron from this shell but also by a Coster–Kronig transition from the L_I- or L_{II}-subshell. These transitions feed the magnetic substates statistically. Therefore the measured alignment has to be corrected for this contribution by multiplying the alignment parameters with the factor $\kappa(b)$ which varies with the impact parameter b (Jitschin *et al* 1982).

$$\kappa(b) = 1 + f_{23}\frac{I_{L_{II}}(b)}{I_{L_{III}}(b)} + (f_{12}f_{23} + f_{13})\frac{I_{L_I}(b)}{I_{L_{III}}(b)}. \tag{9}$$

For the present collision system this is only a small correction ($1.04 < \kappa(b) < 1.09$).

The alignment parameter $A_{22}^{\text{lab}}(b)$ was obtained from the azimuthal angular dependence of the L_l-line intensity at $\vartheta = 90°$ evaluating the ratio of true to random coincidences for the different sectors of the PPAD . Because of the low count rate the 16 sectors had to be reduced to four quarters and several impact parameter regions (i.e. rings on the PPAD) had to be combined, too.

3. Results and discussion

3.1. Ionization probabilities

The ionization probability for the total L-shell is shown in figure 5. The different symbols for the data points denote three different measurements at different target–PPAD distances.

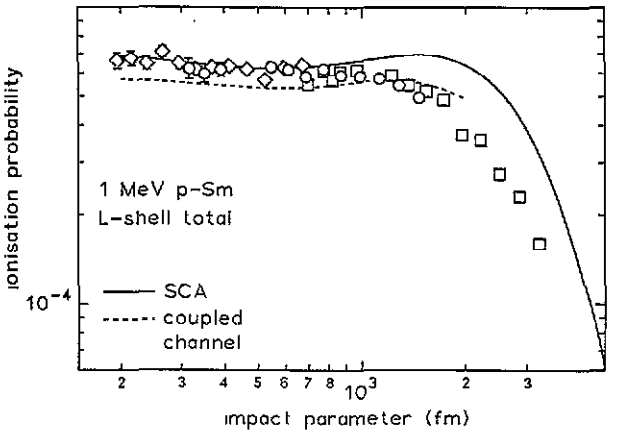

Figure 5. Ionization probability of the Sm L-shell (all subshells). Full curve, SCA (frozen orbitals); broken curve, coupled channel calculation.

The error bars include only the statistical error. In one of the experiments the absolute value of the ionization probability was measured as described in the experimental section. The three data sets have a broad overlap in the covered impact parameter range and could therefore be connected to each other.

The SCA calculations shown in the figure are based on relativistic hydrogen like wavefunctions. They are performed using the SCA code by Trautmann and co-workers (1985). The binding energies of the united atom system are used for the binding correction. The calculations are in good agreement with the data for small impact parameters but overestimate the data for large impact parameters. Such deviations of the SCA from the experimental data have been observed for 0.9 MeV u^{-1} He^+ on Pt, Ne^{3+} on Pt and Yb (Dexheimer *et al* 1986), too. The overestimate by the SCA at large impact parameters might only partially be due to the use of hydrogen-like wavefunctions. We discuss below also the effect of 'frozen orbitals' in the theoretical model. For the largest measured impact parameters the use of the united atom wavefunctions is questionable and the use of the separated atom binding energy might be more reasonable. However, this would increase the calculated probability even more. Also shown are the results of coupled channel calculations by Mehler and co-workers (1985a, b). These calculations included about 5000 different reaction channels. They use the same assumption of 'frozen orbitals' but are based on HFS wavefunctions for the united atom system.

For the L_I-subshell the results of the coupled channel calculations are in good agreement to the experimental data in the relative shape as well as in the absolute height over the whole impact parameter range (figure 6). The relative shape of the ionization probability is also well predicted by the SCA.

The increase of the L_I ionization probability towards small impact parameters can be explained as follows. At small distances from the nucleus the electrons have in average higher momenta than at large distances. This can lead to a self-ionization by scattering the electron off the projectile particularly at small v_p. For 1 MeV p $\rightarrow$ Sm the projectile velocity is about three times smaller than the mean L_I-shell electron velocity. Relativistic effects enhance this 'self-ionization' process even more (Ullrich *et al* 1986). For the $L_{II,III}$-subshells the contribution of this 'self-ionization' effect is much reduced due to the node of the wavefunction at the origin. Thus despite the higher binding energy for the L_I-subshell compared to the $L_{II,III}$-subshell the ionization probability for the L_I-subshell can

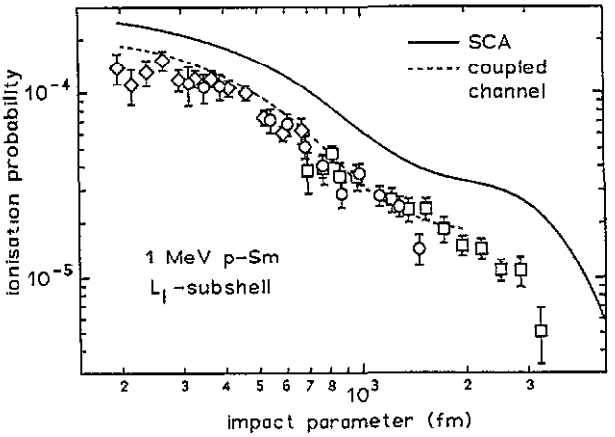

Figure 6. Ionization probability of the L_I-subshell. Full curve, SCA (frozen orbitals); broken curve, coupled channel calculation.

reach the ionization probability of the L_{II}- or L_{III}-subshell at small impact parameters. The structure in the L_I-subshell ionization probability around 1300 fm is due to the node in the L_I wavefunction.

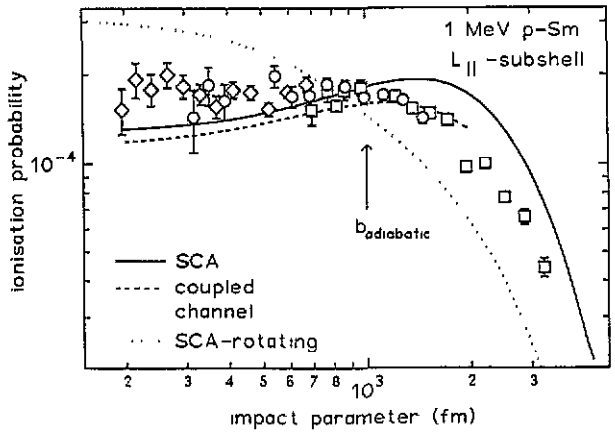

Figure 7. Ionization probability of the L_{II}-subshell. Full curve, SCA (frozen orbitals); dotted curve, SCA (rotating orbitals); broken curve, coupled channel calculation (frozen orbitals).

The ionization probabilities for the L_{II}- and L_{III}-subshell are shown in figures 7 and 8. In contrast to the situation for the L_I-subshell severe discrepancies between the experimental data and the SCA results as well as the coupled channel calculation are observed also for the shape of the impact parameter dependence. Towards small impact parameters both theories predict an about 25% decrease of the ionization probability which is not visible in the data. This discrepancy between experiment and both theoretical predictions cannot be due to vacancy sharing between the L-subshells since this effect of intra-shell transitions is included in the coupled channel calculations. For large impact parameters these discrepancies become much more severe, the SCA calculation overestimates the ionization probabilities for the L_{II} and the L_{III} subshell by nearly a factor of two as it could already be seen in the total L-shell

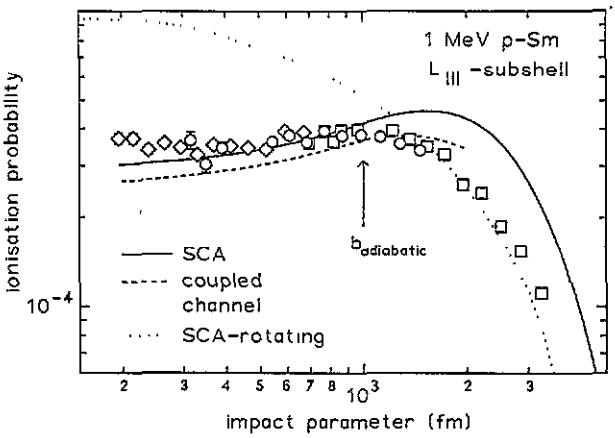

Figure 8. Ionization probability of the L_{III}-subshell. Curves, as figure 7.

ionization probability. As outlined in the introduction the collision system 1 MeV p → Sm was chosen because of its very low ionization probability. The ionization probability of 0.04% for all L_{III} electrons corresponds to a probability of 0.01% per electron to be ionized. Since the ionization probability is a direct measure of the perturbation strength, one could expect perturbation theory to work well here. A similar discrepancy between experimental and SCA L-subshell ionization probabilities at large impact parameters was already found for collision systems with larger perturbation strength (Dexheimer *et al* 1986).

In order to discuss the possibility of a quasiadiabatic rotation of the wavefunction one has to compare the angular velocity of the rotation of the internuclear axis ω_{int} with the electron velocity. For a straight-line trajectory ω_{int} at the distance of closest approach is given by v_{pro}/b. In the classical Bohr model the electron angular velocity for the Sm L-shell is about 320 au. For 1 MeV protons one obtains that at an impact parameter $b_{adiabatic}$ of about 1000 fm the angular velocity at the distance of closest approach is about equal to the classical angular velocity of the electron. Therefore for impact parameters much smaller than 1000 fm the Sm L-shell electrons are too slow to follow the rapidly rotating internuclear axis. For these impact parameters the 'frozen orbital basis' should be adequate to describe the problem. At larger impact parameters, however, an adiabatic rotation can be expected. In the case of 'rotating orbitals' the ionization probability will be reduced since the electrons dodge the perturbation by the projectile.

Legrand and co-workers (1992) have performed SCA calculations with fully adiabatic rotating wavefunctions (Legrand *et al* 1992). The results are shown by the dotted lines in figures 7 and 8. At large impact parameters these results show the expected reductions of the ionization probability. For the L_{III}-subshell these adiabatic calculations are for $b > b_{adiabatic}$ in good agreement with the data while for the L_{II}-subshell the data are in between the adiabatic and non-adiabatic SCA. For impact parameters below 1000 fm the adiabatic model is unrealistic as discussed above. Therefore for $b < b_{adiabatic}$ the SCA with 'frozen orbitals' yields the better description of the experimental data. While for $b > b_{adiatbatic}$ the calculation with 'frozen orbitals' overestimated the total L-shell ionization probability (figure 5) as well as the ionization probability for the $L_{II,III}$ subshells by up to a factor of two.

3.2. Alignment

The alignment of the L_{III}-subshell should provide a very stringent test for the models of rotating or frozen orbitals. Experimentally, however, the alignment parameters are very

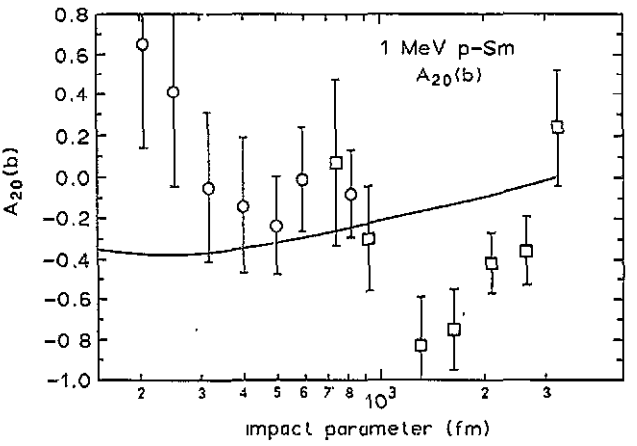

Figure 9. Alignment parameter A_{20}. Full curve, SCA (frozen orbitals).

hard to determine since they have to be extracted from the angular distribution of the very weak L_l line (using equation (8)). The alignment parameter $A_{20}(b)$ is defined as follows:

$$A_{20}(b) = \frac{I_{m_j=3/2}(b) - I_{m_j=1/2}(b)}{I_{m_j=3/2}(b) + I_{m_j=1/2}(b)}. \tag{10}$$

The alignment parameter $A_{22}(b)$ is proportional to the expectation value of angular momenta in the x and y directions (Blum and Kleinpoppen 1979) (z is given by the beam direction)

$$A_{22}(b) \sim \langle L_x^2 - L_y^2 \rangle. \tag{11}$$

As mentioned in the experimental section the alignment parameters are dependent on the reference frame. The experimental results for $A_{20}(b)$ (figure 9) and $A_{22}(b)$ (figure 10) are given in the laboratory frame. Very poor agreement between theory using frozen orbitals and the experimental data is observed for both alignment parameters. The effect of a possible adiabtic rotation of the wavefunction on the alignment has to be discussed in two steps.

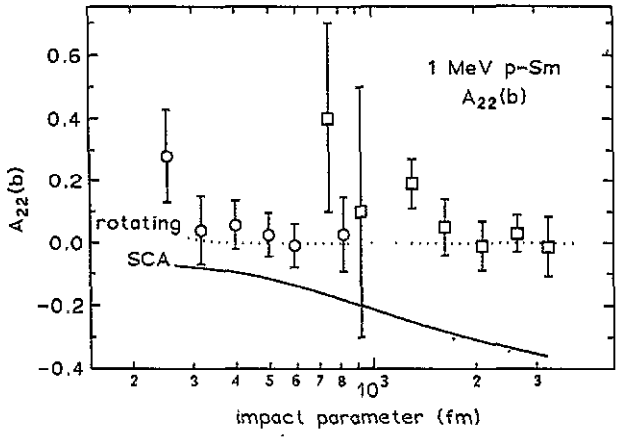

Figure 10. Alignment parameter A_{22}. Full curve, SCA (frozen orbitals); dotted curve, rotating orbitals.

In a first step the alignment can be estimated seen in the rotating frame at the time of the creation of the vacancy. In this reference frame one would expect a negative value for A_{20}^{rot} (i.e. a higher ionization probability for the $m_j = \pm\frac{1}{2}$ than for the $m_j = \pm\frac{3}{2}$ subshell) since the projectile trajectory passes only the $m_j = \pm\frac{1}{2}$ orbital and does not touch the $m_j = \pm\frac{3}{2}$ (see figure 1). In the non-adiabatic SCA such a projectile path along the quantization axis can be simulated by choosing $b = 0$. For this impact parameter the SCA prediction is $A_{20}^{SCA}(b = 0) = -0.55$. This value is only a lower limit for the alignment since for larger impact parameters the alignment has to go to zero. In the adiabatic case the system is rotationally symmetric around the z-axis at all times. This leads necessarily to $A_{22}^{\text{rot}} = 0$ (see equation (11)) (Berinde *et al* 1984).

In a second step one has to transform A_{KQ}^{rot} to the laboratory frame. The radiative decay of the L-vacancy takes place long after the collisions. Since the experimental alignment parameters are obtained from the anisotropy of the x-ray emission they reflect the alignment long after the collision and not at the time of the creation of the vacancy. After the collision the z-axis of the rotating coordinate frame is given by the direction of the outgoing projectile. As discussed above adiabaticity is a reasonable assumption only for large impact parameters, i.e. very small scattering angles where the rotational frame at the time of the decay is nearly equal to the laboratory frame and therefore $A_{KQ}^{\text{rot}} \approx A_{KQ}^{\text{lab}}$.

The experimental data for A_{20} and for impact parameters between 1000 and 3000 fm are much more negative than predicted by the non-adiabatic SCA. This is in agreement with what can be expected in the case of an adiabatic rotation. In addition the experiment shows in contradiction to the SCA predictions nearly no azimuthal angular anisotropy of the L_l line for all impact parameters, i.e. $A_{22} \approx 0$. This is consistent with the assumption of fully adiabatic rotation of the quantization axis. Similar conclusions in favour of the model of rotating orbitals were already drawn by (Palinkas *et al* 1980) and (Jitschin *et al* 1982) on the basis of the projectile energy dependence of the total alignment (see also Rösel *et al* 1982).

3.3. Vacancy sharing

Several studies as well on total L-subshell ionization cross sections as on the impact parameter dependence of the L-subshell ionization probabilities investigated the mixing of the L-subshells due to the perturbation by the projectile. These intra shell transitions lead to a statistical distribution of the vacancies between the L-subshell which is independent of the impact parameter. Figure 11(a) shows the ratio of the ionization probabilities of the L_{III}-subshell to the L_I-subshell. The ratio varies by about a factor of eight with the impact parameter. For impact parameters above 400 fm the strong b dependence of the $I_{L_{III}}(b)/I_{L_I}(b)$ ratio indicates that there is no vacancy sharing for 1 MeV p → Sm. This strong b dependence is well predicted by the SCA, i.e. by a first-order theory which does not account for the mixing of the L-subshell. The coupled channel calculation as shown by the broken curve in figure 11(a) fully accounts for this higher order effect. Since this calculation does not predict any mixing for 1 MeV p impact even below 400 fm the constancy of the experimental ratio below 400 fm cannot be interpreted as an indication for vacancy sharing.

For comparison figure 11(b) shows the same ratio for 4 MeV p impact from Zehendner *et al* (1987). For this higher energy the ratio becomes completely independent of the impact parameter and close to the statistical distribution value of two.

Table 1 lists the collision systems for which the impact parameter dependence of the L-subshell have been reported so far. As a measure of the perturbation strength the total L-shell ionization probability at an impact parameter $b = 200$ fm is listed. The comparison

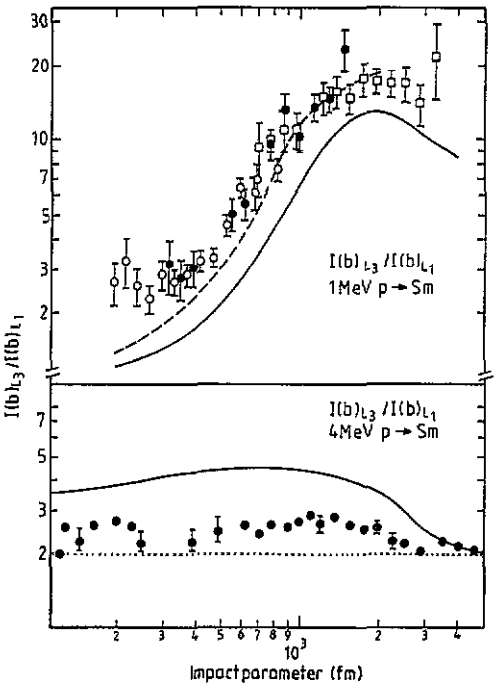

Figure 11. Ratio L_{III}/L_I of the L-subshell ionization probabilities. (*a*) 1 MeV p impact, this work: full curve, SCA; broken curve, coupled channel calculation. (*b*) 4 MeV p impact, data from Zehendner *et al* (1987): full curve, SCA; broken curve, statistical distribution.

Table 1. L-subshell vacancy sharing.

Energy	System	$I(b)_{L_{tot}}$ $b = 200$ fm	Vacancy sharing	Reference
2.3 MeV u^{-1}	Ar → Au	$\approx 10^{-1}$	Complete	Schadt *et al* (1988)
0.9 MeV u^{-1}	He^{1+} → Pt	$\approx 10^{-3}$	None	Dexheimer *et al* (1986)
0.9 MeV u^{-1}	Ne^{3+} → Pt	$\approx 10^{-2}$	Partial	Dexheimer *et al* (1986)
0.9 MeV u^{-1}	Ne^{3+} → Yb	$\approx 3 \times 10^{-2}$	Complete	Dexheimer *et al* (1986)
4 MeV	p → Sm	$\approx 5 \times 10^{-3}$	Partial	Zehendner *et al* (1987)
1 MeV	p → Sm	$\approx 7 \times 10^{-4}$	None	This work

shows that the effect of intra-shell transitions depends on the perturbation strength and not only on the projectile charge.

4. Conclusions

Absolute L-subshell ionization probabilities and the alignment parameters A_{20} and A_{22} have been measured for a collision system where the perturbation is extremely small. For this case SCA can be tested with high accuracy. Surprising discrepancies between the experimental data and SCA with stationary states which are aligned along the incoming beam axis are found for the ionization probabilities of the non spherical symmetric subshells. Very poor agreement for the alignment parameters is found. At impact parameters where the velocity of the electrons is larger than the rotation velocity of the internuclear axis SCA calculations with

adiabatically rotating wavefunctions improve agreement between theory and experiment. We have shown that even for very asymmtric collision systems with extremly small ionization probabilities it is necessary to go beyond first-order pertubation theory and include the adiabatic effect of the rotating internuclear axis on the ionization probabilities and the alignment.

Acknowledgments

This work was supported by DFG and BMFT. We are indebted to Gerhard Mehler for providing the coupled channel calculations and Dirk Trautmann for performing the SCA calculations. Special thanks also to Tibor Papp for patient discussions about alignment tensors.

References

Andersen J U, Kocbach L, Laegsgaard E, Lund M and Moak C D 1976 *J. Phys. B: At. Mol. Phys.* **9** 3247
Andersen J U, Laegsgaard E and Lund M 1982 *Nucl. Instrum. Methods* **192** 79
Andreamonje S, Chemin J F, Roturier J F, Scheurer J N 1981 *Z. Phys.* A **300** 31
Bauer K G, Fazly Q, Mommsen H and Schurkess P 1978 *J. Phys. B: At. Mol. Phys.* **11** 4227
Berezkho E G and Kabachnik N M 1977 *J. Phys. B: At. Mol. Phys.* **10** 2467
Berinde A, Ciortea C, Enulescu A, Fluerasu D, Piticu I and Zoran V 1984 *Nucl. Instrum. Methods* B **4** 283
Blum K and Kleinpoppen H 1979 *Phys. Rep.* **52** 251
Brandt W, Laubert R and Sellin I 1966 *Phys. Rev.* **56** 151
Bräuning H, Ullmann K, Dangendorf V, Schmidt-Böcking H, Trautmann D and Kauer Th 1991 *Phys. Rev.* A **44** 2868
Cheng-Ming Fou, Kraftel M V, Benck E C, Rösel F and Trautmann D 1983 *J. Phys. B: At. Mol. Phys.* **16** 1409
Dexheimer K, Ullrich J, Stiebing K E, Schadt W, Kelbch S, Kelbch C, Schuch R, Zehendner S and Schmidt-Böcking H 1986 *J. Phys. B: At. Mol. Phys.* **19** 3086
Dost M, Hoppenau S, Kising J, Röhl S and Schorn P 1985 *Phys. Rev.* A **24** 693
Gruber G 1983 *PhD Thesis* University Frankfurt
Hagmann S, Cocke C L, McDonald J R, Richard P, Schmidt-Böcking H and Schuch R 1982 *Phys. Rev.* A **25** 1918
Hansen J P, Kocbach L, Dubois A and Nielsen S E 1990 *Phys. Rev. Lett.* **64** 2491
Hansteen J M, Kocbach L and Graue A 1985 *Phys. Scr.* **31** 63
Jakob A 1985 *PhD Thesis* University of Basel
Jitschin W, Kaschuba A, Hippler R and Lutz H O 1982 *J. Phys. B: At. Mol. Phys.* **15** 763
Konrad J, Schuch R, Hoffmann R and Schmidt-Böcking H 1984 *Phys. Rev. Lett.* **52** 188
Krause M O 1979 *J. Phys. Chem. Ref. Data* **8** 307
Laegsgaard E, Andersen J U and Lund M 1974 *Proc. Int. Conf. on X-Ray Processes in Matter (Phys. Fenn.* **9** suppl 1) p 52
Legrand I, Dörner R, Schmidt-Böcking H and Zoran V 1991 *Proc. 4th Workshop on High-Energy Ion–Atom Collisions (Debrecen)* (Lecture Notes in Physics 376) ed D Berenyi and G Hock (Berlin: Springer) p 312
Legrand I C, Zoran V, Dörner R, Schmidt-Böcking H, Berinde H A, Fluerasu D and Ciortea C 1992 *J. Phys. B: At. Mol. Opt. Phys.* **25** 189
Mehler G, de Reus T, Müller U, Reinhardt J, Müller B, Greiner W and Soff G 1985 *Nucl. Instrum. Methods* A **240** 559
Mehler G, de Reus T, Soff G and Müller U 1985 *Z. Phys.* A **320** 355
Nolte G, Schadt W, Janke M, Roller Z, Schneider D and Schmidt-Böcking H 1984 *Nucl. Instrum. Methods* B **2** 346
Palinkas J, Sakardi L and Schlenk B 1980 *J. Phys. B: At. Mol. Phys.* **13** 3829
Rösel F, Trautmann D and Bauer G 1982 *Nucl. Instrum. Methods* **192** 43
Salin A 1990 *Phys. Rev. Lett.* **65** 2474
Schadt W, Schmidt-Böcking H, Nolte G, Roller Z, Skutlatz Z A, Wassermann M and Zschornack G 1988 *Z. Phys.* D **8** 271

Schmidt-Böcking H, Schadt W and Kelbch S 1983 *Fundamental Processes in Energetic Atomic Collisions* ed H O Lutz (New York: Plenum)

Schmidt-Böcking H, Schule R, Stiebing K E, Bethge K, Tserruya I and Zekl H 1977 *J. Phys. B: At. Mol. Phys.* **10** 2663

Schmidt-Böcking H, Stiebing K E, Schadt W, Löchter N, Gruber G, Kelbch S, Bethge K, Schuch R and Tserruya I 1982 *Nucl. Instrum. Methods* **192** 71

Scofield J H 1974 *At. Data Nucl. Data Tables* **14** 121

Steinbauer E and Benka O 1989 *J. Phys. B: At. Mol. Opt. Phys.* **22** 2011

Stiebing K E, Schmidt-Böcking H, Schule H, Bethge K and Tserruya I 1976 *Phys. Rev.* A **14** 146

Trautmann D, Rösel F and Bauer G 1985 *J. Phys. B: At. Mol. Phys.* **1167** 18

Ullrich J, Dangendorf V, Dexheimer K, Do K, Hagmann S, Kelbch C, Kelbch S, Rösel F, Schadt W, Schmidt-Böcking H, Stiebing K E and Trautmann D 1986 *Z. Phys.* D **2** 137

Zehendner S, Baptista G B, Dörner R, Justiniano E, Konrad J, Schmidt-Böcking H and Schuch R 1987 *Z. Phys.* D **4** 243